JACS
JOURNAL OF THE AMERICAN CHEMICAL SOCIETY
Article
pubs.acs.org/JACS

Mechanosensitive Gold Colloidal Membranes Mediated by Supramolecular Interfacial Self-Assembly

João Paulo Coelho,[†] María José Mayoral,[‡] Luis Camacho,[§] María T. Martín-Romero,[§] Gloria Tardajos,[†] Iván López-Montero,[†,#] Eduardo Sanz,[†] David Ávila-Brande,[⊥] Juan José Giner-Casares,*[,§] Gustavo Fernández,*[,∥] and Andrés Guerrero-Martínez*[,†]

[†]Departamento de Química Física I, Universidad Complutense de Madrid, Avda. Complutense s/n, 28040 Madrid, Spain

[‡]Nanostructured Molecular Systems and Materials Group, Departamento de Química Orgánica, Facultad de Ciencias, Universidad Autónoma de Madrid, 28049 Madrid, Spain

[§]Departamento de Química Física y Termodinámica Aplicada, Universidad de Córdoba, Campus de Rabanales, Edificio Marie Curie, 14014 Cordoba, Spain

[#]Instituto de Investigación Hospital 12 de Octubre i+12, Avda. de Córdoba s/n, 28041 Madrid, Spain

[⊥]Departamento de Química Inorgánica I, Universidad Complutense de Madrid, Avda. Complutense s/n, 28040 Madrid, Spain

[∥]Organisch-Chemisches Institut, Westfälische Wilhelms-Universität Münster, Corrensstraße, 40, 48149 Münster, Germany

Supporting Information

ABSTRACT: The ability to respond toward mechanical stimuli is a fundamental property of biological organisms at both the macroscopic and cellular levels, yet it has been considerably less observed in artificial supramolecular and colloidal homologues. An archetypal example in this regard is cellular mechanosensation, a process by which mechanical forces applied on the cell membrane are converted into biochemical or electrical signals through nanometer-scale changes in molecular conformations. In this article, we report an artificial gold nanoparticle (Au NP)−discrete π-conjugated molecule *hybrid system* that mimics the mechanical behavior of biological membranes and is able to self-assemble into colloidal gold nanoclusters or membranes in a controlled and reversible fashion by changing the concentration or the mechanical force (pressure) applied. This has been achieved by rational design of a small π-conjugated thiolated molecule that controls, to a great extent, the hierarchy levels involved in Au NP clustering by enabling reversible, cooperative non-covalent ($\pi-\pi$, solvophobic, and hydrogen bonding) interactions. In addition, the Au NP membranes have the ability to entrap and release aromatic guest molecules reversibly (K_b = 5.0 × 10^5 M^{-1}) for several cycles when subjected to compression−expansion experiments, in close analogy to the behavior of cellular mechanosensitive channels. Not only does our hybrid system represent the first example of a reversible colloidal membrane, but it also can be controlled by a dynamic mechanical stimulus using a new supramolecular surface-pressure-controlled strategy. This approach holds great potential for the development of multiple colloidal assemblies within different research fields.

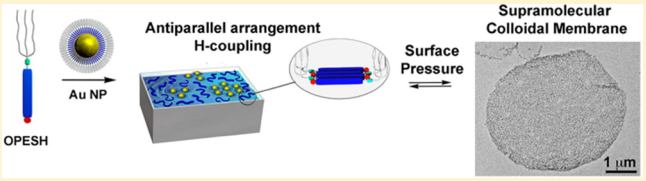

INTRODUCTION

The exploitation of colloidal nanoparticles' self-assembly to produce superstructures with as-yet undefined properties attributable to the new size scale is one of the greatest challenges in the broad field of colloid chemistry.[1] One of the main conceptual approaches for the development of nanoparticle (NP) ensembles has focused on mimicking molecular amphiphilic organizations, ranging from micelles or vesicles to more complex self-assembled structures[2] such as NP clusters, colloidosomes, and liquid crystals.[3−5] As remarkable bioinspired superstructures, colloidal membranes (CMs),[6] consisting of layers of NPs whose assembly is dictated by planar interfaces between two immiscible phases,[7] have recently emerged as excellent mimetic candidates for amphiphilic self-assembly. Colloidal nanoscopic interactions between the constituent NPs at such interfaces lead to a high degree of mesoscopic complexity,[8] mainly characterized by the presence of structural defects, defined morphologies, and self-limited sizes in CMs,[9] which differentiates them from the more conventional highly ordered NP superlattices.[10] For non-amphiphilic systems, the construction of CMs requires the stabilization and trapping of NPs at the interface by entropy-driven self-assembly processes. This results in membranes with mechanical properties analogous to those of lipid bilayers in water.[11] Under such planar interfacial conditions, monodisperse microstructures with disk-shaped NP organizations are obtained as the main geometry.[12]

Despite the recent efforts toward stable CMs, no attention has been paid to the reversibility of the ensembles, an appealing

Received: September 9, 2016
Published: December 30, 2016

DOI: 10.1021/jacs.6b09485
J. Am. Chem. Soc. 2017, 139, 1120−1128

Scheme 1. (a) Molecular Structure of the Thiolated OPE Derivative (OPESH) and Tentative Model Depicting Its Antiparallel Arrangement within Au CCs, and (b) Cartoon Representation of the Compression-Controlled Self-Assembly Modes of OPESH at the Air/Liquid Interface in Isolation (Bottom) and in the Presence of Modified Au NPs (Top)[a]

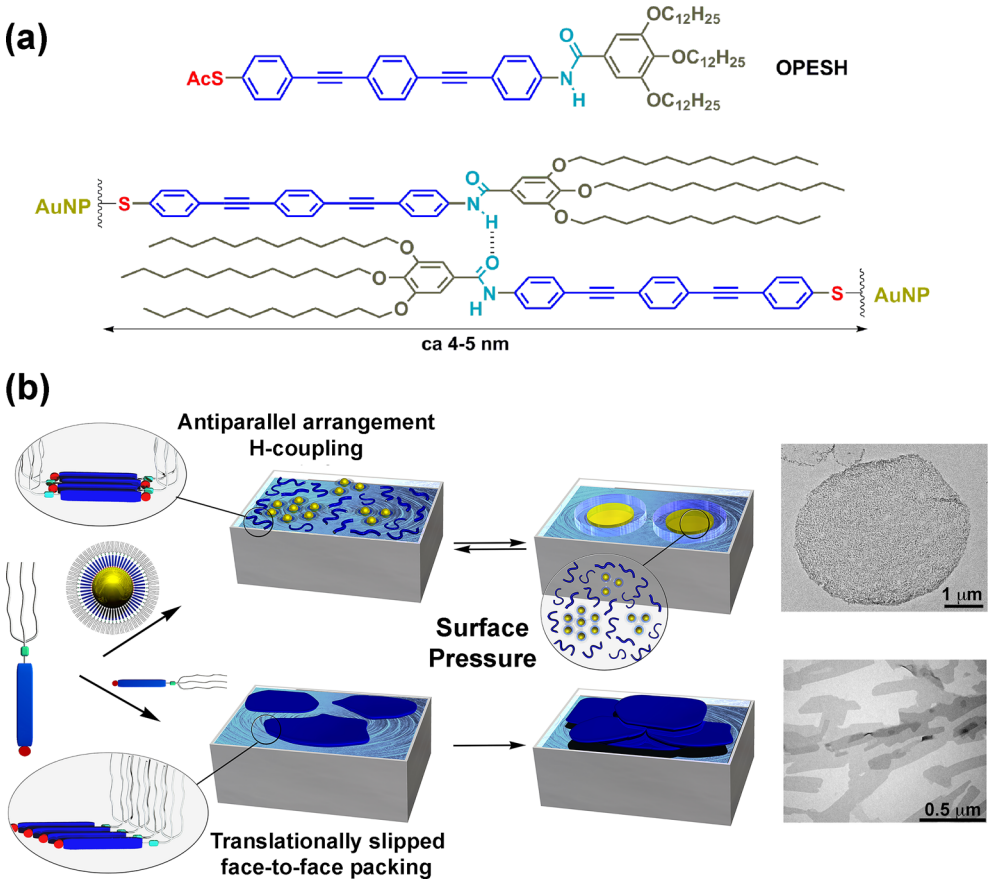

[a]In the presence of Au NPs, a reversible transition from supramolecular gold colloidal clusters to membranes is observed.

property to understand the interactions between colloids, NPs, and proteins once incorporated to the interface.[13−16] This type of dynamic concept has been key to understanding the self-assembly of membrane proteins to form highly ordered functional structures within the cell membrane upon external stimuli.[17] For example, ion channels on membrane cells are reversible protein superstructures whose closed (assembled) and open (disassembled) configurations can be triggered by chemical or electrical signals, temperature, or even mechanical forces.[18]

As a transversal concept, reversibility is the focus of intense research in the field of supramolecular chemistry[19] due to its key role in the bottom-up fabrication of new molecular materials.[20,21] For instance, self-assembled systems have been exploited to confer reversibility to NP and protein ensembles with different morphologies.[22−24] As notable examples, colloidal gold nanoparticles (Au NPs) have shown remarkable versatility toward supramolecular functionalization, allowing their reversible assembly into various superstructures.[25,26] Along these lines, we have recently demonstrated that cooperative supramolecular polymerization processes[27] can be transferred from small molecules to Au NPs,[28] a process that has shown high levels of reversibility with temperature. Therefore, a supramolecular strategy appears to be most suited to obtain reversible CMs by functionalizing Au NPs with rationally designed supramolecular interactive ligands.

Inspired by these precedents, and considering that the Langmuir technique offers the possibility of arranging supramolecules[29] and NPs[30,31] into highly ordered mono- and multilayers at the air/liquid interface, we propose herein an unprecedented surface-pressure-controlled supramolecular strategy to obtain reversible mechanosensitive gold colloidal membranes (Au CMs) with self-limited thickness and two-dimensional (2D) extent at the nanoscopic and microscopic levels, respectively. In particular, we have prepared interfacial colloidal suspensions containing Au NPs and supramolecular aggregates acting as dispersed and semicontinuous phases, respectively. Under mild surface compression as the external mechanical stimulus, Au NPs undergo a reversible transition from small gold colloidal clusters (Au CCs) to microsized disk-shaped Au CMs, while the supramolecular self-assembly at the semicontinuous phase remains intact (Scheme 1).

We propose a mechanistic interpretation based on the arrangement of the supramolecular aggregates in the presence of nanocrystals, where the NP molecular corona acts as a supramolecular nucleation surface, promoting the entrapment of the supramolecular phase and the clustering of the Au NPs. Therefore, Au CCs are spontaneously reorganized into larger Au CMs to minimize the free energy when the concentration of nanocrystals per area increases. This explanation is supported by the changes the supramolecular phase experiences in its aggregation structure at the molecular level, from translationally slipped face-to-face aggregates with a slightly twisted dye

DOI: 10.1021/jacs.6b09485
J. Am. Chem. Soc. 2017, 139, 1120−1128

arrangement to H-type antiparallel-arranged systems in the absence and presence of Au NPs, respectively.[32−34] Moreover, the transition from Au CCs to Au CMs shows mechanosensitive reversibility due to an entropy contribution that may prevail at low Au NP surface concentrations. The cooperative character of the non-covalent interactions that control the self-assembly behavior of Au NPs and supramolecular aggregates,[28] mainly cooperative $\pi-\pi$ and hydrogen bonding,[35] allows for the reversibility of the Au CM formation. Finally, so as to exploit this mechanosensitive function,[21] the Au CMs were used as host matrices for highly hydrophobic molecules that can be reversibly entrapped and released via dynamic self-assembly, demonstrating the potential of these superstructures as molecular harvesters and pressure-controlled release systems.

RESULTS AND DISCUSSION

Supramolecular Self-Assembly of Gold Colloidal Membranes. A rational strategy toward stable and processable Au NP assemblies consists in the exploitation of reversible non-covalent forces. Discrete π-conjugated ligands with an extended aromatic surface are ideal candidates in this regard due to their ability to π-stack in a predictable fashion,[36,37] which can be reinforced by cooperative non-covalent interactions such as hydrogen bonding, dipolar, or metal−metal interactions.[36,38] On this basis, we synthesized a discrete oligomeric fragment derived from oligophenyleneethynylene (OPE)[39−48] substituted on one end with a thioacetate group and on the opposite end with a 3,4,5-tris(dodecyloxy)-*N*-benzamide functional group (Scheme 1a; for synthesis and ligand replacement see the Supporting Information). While the former should ensure the coordination to Au NPs (10.5 ± 1.3 nm average in diameter, Figure S1) through Au−S bonding,[27] the latter is expected to introduce an additional driving force for self-assembly, i.e., cooperative hydrogen bonding between the amide moieties and solvophobic interactions involving the alkoxy chains. On the other hand, the choice of ligand relies on the well-known supramolecular, optical, and electronic properties of OPEs,[49] which will enable the investigation of the photophysical properties of the functionalized Au NPs[27] by various spectroscopic methods *in situ* at the air/liquid interface.

The studied thiolated OPE derivative (OPESH, Scheme 1a) exhibits amphiphilic behavior at the air/water interface using chloroform as the spreading agent. The spontaneous formation of flakes at surface concentrations of 1.3×10^{-10} mol/cm^2 is evident from the transmission electron microscopy (TEM) micrographs of the interface obtained by dip-coating (Scheme 1b, bottom right, and Figure 1a). The regular morphology of the flakes points to intense and directional non-covalent interactions between OPESH molecules within the self-assembled supramolecular aggregates. In contrast, the co-spreading of free OPESH molecules together with the modified gold nanoparticles (OPES-Au NPs) noticeably changes the self-assembly pattern at the air/water interface. Figure 1b depicts the morphology of the interfacial structure of a mixed film comprising both free OPESH molecules and OPES-Au NPs. The surface concentration of free OPESH molecules is 1.3×10^{-10} mol/cm^2, in combination with OPES-Au NPs at a surface concentration of 2.9×10^{-14} mol/cm^2. Thus, the surface molar ratio of free OPESH/OPES-Au NPs is 4.5×10^3. In the presence of Au NPs, a semicontinuous sheet phase of OPESH aggregates is observed around homogeneously distributed Au CCs of 5−15 hexagonally packed Au NPs (insets in Figure 1b). The minimum distance between the surfaces of neighboring

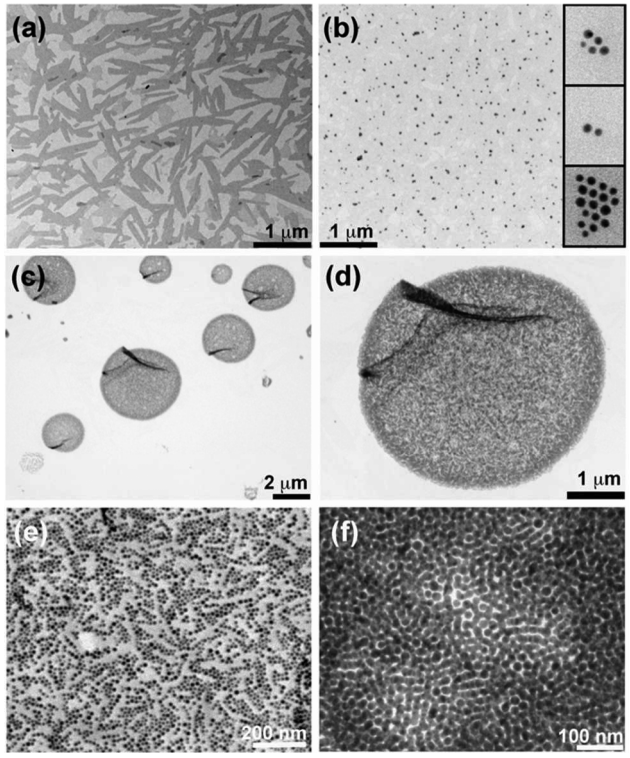

Figure 1. (a) TEM micrograph of the OPESH self-assembled film at the air/water interface (surface concentration of 1.3×10^{-10} mol/cm^2) obtained by dip-coating. (b,c) TEM micrographs of supramolecular Au CCs and Au CMs within the supramolecular phase, respectively. (d) Magnification of an individual Au CM from image (c). The insets in (b) show typical Au CCs formed by hexagonally packed nanocrystals. (e,f) Details of a microsized Au CM and its interior, respectively, where coexistence of Au CCs and supramolecular aggregates is observed (vitrified-like structure).

OPES-Au NPs within the clusters is 4.4 ± 0.5 nm, which approximately corresponds to the length of the geometry-optimized structure of OPESH assuming a fully outstretched conformation of the alkyl chains. This result suggests that OPES-Au NPs self-assemble into Au CCs through the interdigitation of stabilizing agents at the interparticle gaps. Considering the length and functional groups of the OPESH ligand, two areas of interaction within the molecular corona of Au NPs are expected for the clustering process (Scheme 1a): (i) an intermediate region of H-bonding involving the amide functional groups of antiparallel-arranged OPE fragments between Au NPs, and (ii) an area closer to the nanocrystal surface in which $\pi-\pi$ interactions occur due to directionally opposed facing of the extended aromatic backbones and isolated aromatic moieties. Additionally, different configurations at the alkyl chain level are plausible, most likely stabilized by solvophobically driven aryl−alkyl and/or alkyl−alkyl interactions (see dimer in Scheme 1a), as recently observed for OPE-based hydrophobic metal complexes.[50]

The interfacial picture noticeably changes upon increasing the surface concentration of OPESH and OPES-Au NPs up to 1.3×10^{-9} and 2.9×10^{-13} mol/cm^2, respectively, maintaining a constant surface molar ratio of 4.5×10^3. Co-spreading of both components results in the spontaneous formation of 1−5 μm wide disk-shaped Au CMs within the supramolecular phase (Figures 1c,d and S2). Compared to the previously described Au CCs, the concentration of the semicontinuous supra-

DOI: 10.1021/jacs.6b09485
J. Am. Chem. Soc. 2017, 139, 1120−1128

molecular sheet was observed to decrease, pointing to the trapping of supramolecular aggregates within the membranes. As clearly shown in Figure 1d, Au CCs self-assemble into Au CMs with a significant amount of cracks, which evidences the solid-like mechanical properties of the membranes. Figure 1e shows an enlarged region of a representative Au CM from Figure 1c, showing a linear network of Au CCs characteristic of dynamically arrested 2D colloidal gels,[51] surrounded by entrapped supramolecular aggregates. The minimum interparticle distance within the clusters is maintained at 4.5 nm, and larger distances between nanocrystals might involve the presence of extended supramolecular aggregates within the Au CMs. Detailed analysis of the crack regions in the TEM micrographs revealed the presence of multilayers of OPES-Au NPs with hexagonal arrangement (Figure 1f), indicating that even in the case of multilayer accumulation, Au NPs are effectively organized by supramolecular interactions between OPESH ligands.

UV−vis reflection spectroscopy allowed the direct analysis of OPESH molecules and OPES-Au NPs located at the air/water interface, giving *in situ* valuable information on the organization, density, and orientation of both systems. We used the optical response of the Au NPs, known as localized surface plasmon resonance (LSPR),[52] as a very sensitive tool to monitor the *in situ* self-assembly of Au NPs through LSPR coupling.[53] Initially, we tested the reflection band of the sheet-like aggregates formed by OPESH in the absence of Au NPs at the air/water interface (Figure 2). Interestingly, the reflection maximum (black spectrum in Figure 2a,b) undergoes a slight hypsochromic shift ($\Delta\lambda = -6$ nm) compared to the absorption spectrum of a molecularly dissolved state recorded in solution (green spectrum in Figure 2b). Additionally, the shoulder at ~365 nm becomes considerably more pronounced for the aggregate spectrum at the air/water interface, whereas the monomer species does not absorb beyond ~380 nm. These spectral signatures suggest face-to-face π-stacking of the OPESH molecules into sheet-like aggregates with a twisted conformation (rotational displacement) of the OPESH molecules within the stack.[54−56] However, significant changes in the OPESH packing modes can be noticed when Au NPs functionalized with OPESH are available at the interface. Figure 2a shows the normalized UV−vis reflection spectra of a mixture of OPESH and OPES-Au NPs under Au CCs and Au CMs formation conditions. The spectra reveal contributions from both molecular (transition at 316 nm) and Au NP (LSPR band at 560 nm) components. In the presence of Au CCs, the reflection band of the OPESH units blue-shifts from 336 to 316, whereas the typical LSPR band of Au NPs broadens and shifts toward high wavelengths up to 600 nm due to strong LSPR coupling (see red spectrum in Figure 2b). This plasmonic effect becomes even more pronounced during the transition from Au CCs to Au CMs due to a stronger interaction between the Au NPs, whereas the OPESH reflection band remains at 316 nm (Figure 2a,b). These results imply almost no significant modifications of the molecular packing of the OPE units when comparing their environment within Au CCs and Au CMs. For both assemblies, the presence of a sharp blue-shifted band relative to that of the monomer species is indicative of an H-type aggregation process. In particular, the sharpening and further blue shift (316 vs 333 nm) of this band in the presence of Au NPs suggests that the spontaneous formation of H-aggregates is promoted by a topological arrangement of the supramolecular phase nucleated at the molecular corona of Au NPs. Such new aggregation pattern induces the clustering of nanocrystals, and therefore the transition from Au CCs to Au CMs to minimize the interfacial free energy when the concentration of nanocrystals per area increases. These results motivated us to investigate the proposed mechanism through the controlled formation of Au CMs at the air/water interface by the Langmuir technique, which allows the fine tuning of the spatial proximity of nanocrystals at the liquid interphase by mechanical compression of the supramolecular nanocrystal layer.

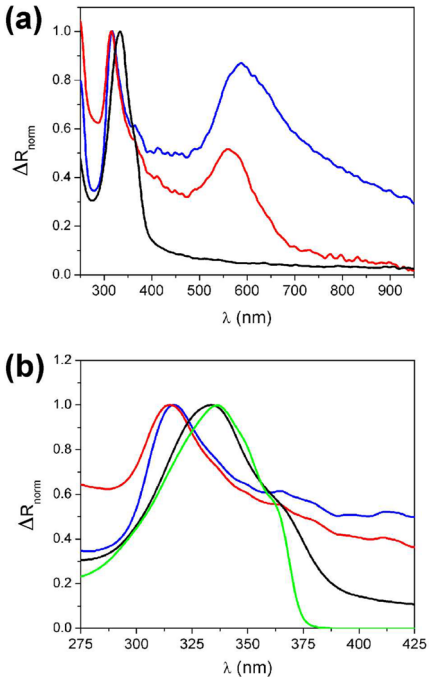

Figure 2. (a) Normalized UV−vis reflection spectra of OPESH (black), Au CCs (red), and Au CMs (blue) recorded *in situ* at the air/water interface. (b) Spectral contributions of the OPESH region in chloroform solution (green), and in the absence (black) and presence of Au NPs (Au CCs (red) and Au CMs (blue)) at the air/water interface, showing their different packing modes as translationally shifted and antiparallel aggregates, respectively.

Mechanosensitive Formation of Supramolecular Gold Colloidal Membranes. The observed solid-like mechanical properties of the spontaneously formed Au CMs suggest the potential suitability of compression−expansion cyclic experiments at the air/water interface (Figure 3) to validate the proposed Au NP concentration-based mechanism. Note that *in situ* monitoring of the NP arrangement at the air/liquid interface usually demands synchrotron-based experimental techniques,[57] whereas Au NP self-assembly can be followed here for the first time in detail using lab-available UV−vis reflection spectroscopy. The cyclic surface pressure−area (π−A) isotherms at the air/water interface of the mixture of OPESH and OPES-Au NPs are shown in Figure 3a (surface conditions identical to those in Figure 1b). The film was compressed to a fixed surface pressure below the collapse (30 mN/m), allowing some stabilization time to avoid kinetic effects (Figure S3). The π−A isotherm of the mixed film was expanded and shifted to larger effective molecular areas compared to that of the pure OPESH under the same surface concentration and compression conditions (Figure 3b), evidencing the presence of OPES-Au NPs at the interface.[58]

DOI: 10.1021/jacs.6b09485
J. Am. Chem. Soc. 2017, 139, 1120−1128

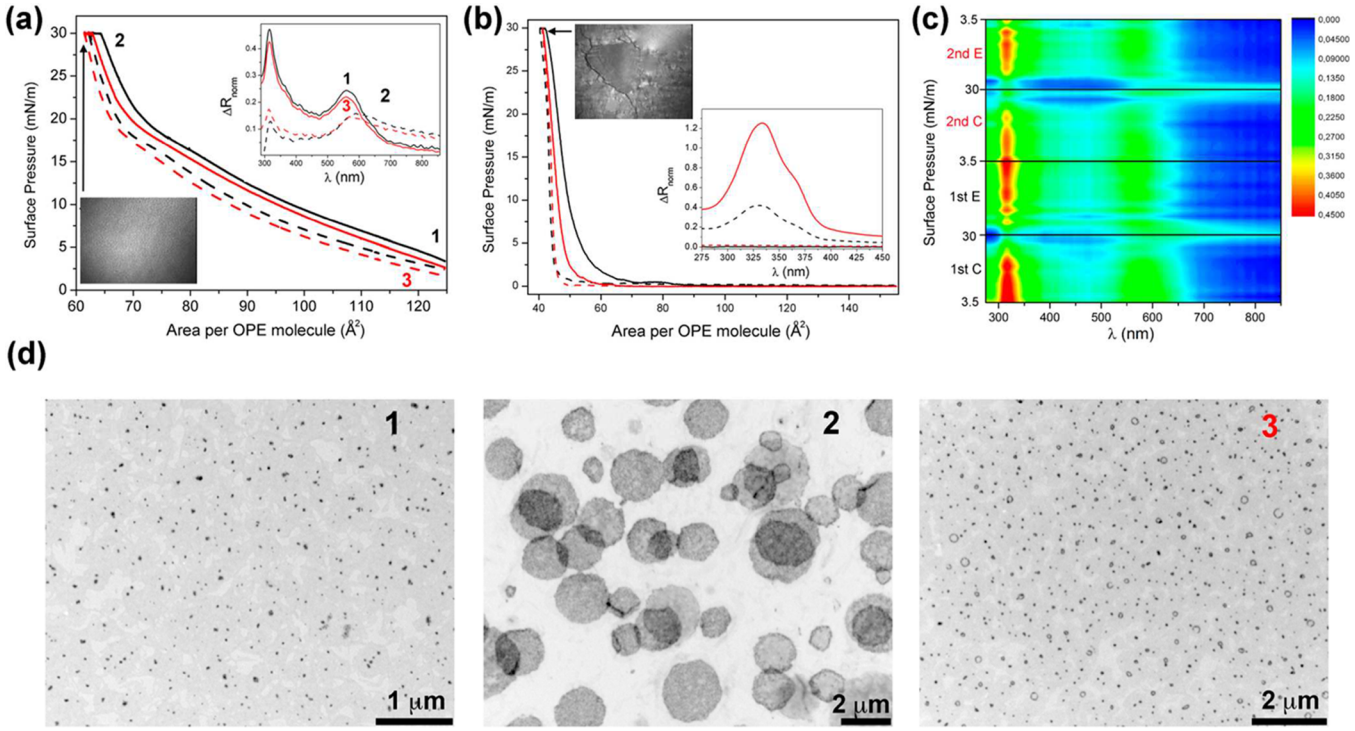

Figure 3. Mechanosensitive reversible response of gold colloidal membranes at the air/water interface. (a) Surface pressure−area isotherms of the mixed OPESH:OPES-Au NP monolayer at surface conditions identical to those in Figure 1b,c. The inset shows the reversible normalized UV−vis reflection spectra of Au CCs (1 and 3), and Au CMs (2) recorded *in situ* at the air/water interface. A representative BAM picture of the Langmuir OPESH:OPES-Au NP monolayer at 30 mN/m is included. (b) Surface pressure−area isotherms of the OPESH monolayer at surface conditions identical to those in Figure 1a. The inset shows the non-reversible normalized UV−vis reflection spectra of the sheet-like aggregates. A representative BAM picture of the Langmuir monolayer of OPESH at 30 mN/m is included. (c) 3D plot of the surface pressure−area isotherms vs the normalized UV−vis reflection spectra of the mixed OPESH:OPES-Au NP monolayer after two compression−expansion cycles. (d) TEM micrographs of the transition from Au CCs (1 and 3) to Au CMs (2) showing the highly reversible mechanosensitive response of the system.

A relevant point is the possible formation of multilayers by the OPESH molecule at the air/water interface. Note that no significant loss of area at 30 mN/m is registered during experiment time. Thus, we discard the contribution of formation of multilayers at 30 mN/m according to the surface pressure−molecular area isotherm shown in Figure 3b. Yet, the possibility of obtaining multilayers of OPESH at higher values of surface pressure and longer times cannot be ruled out.

The normalized UV−vis reflection spectra recorded under compression of the mixture at surface pressures of 0 and 30 mN/m (inset in Figure 3a) show broadening and a red-shift of the LSPR mode due to plasmon coupling between self-assembled Au NPs at the interface (Figure S4). Additionally, no significant changes in the position of the reflection band of OPESH at 316 nm are observed, in good agreement with the H-coupling configuration that OPESH molecules adopt under the conditions for spontaneous Au CM formation (Figure 1b and S5). In contrast, the intensity of the reflection band significantly decreases with the applied surface pressure in the presence of Au NPs. Provided that all the molecules and Au NPs remain at the interface during compression of the mixed film, the decrease in the normalized reflection intensity suggests overall changes in the dipolar orientation of the OPE moieties, while the supramolecular H-aggregate structure remains unaltered. Under the same compression, the position of the normalized reflection band of isolated OPESH remains unchanged at 333 nm, showing significantly different molecular packing in the absence of Au NPs. The observed absence of correlation between the normalized reflection intensity and the surface pressure (inset in Figure 3b), along with the abrupt change of the slope at high areas per OPESH molecule (Figure 3b), point to a non-homogeneous distribution of supramolecular interfacial aggregates over the whole surface, as observed by Brewster angle microscopy (BAM) (Figures S6,S7).

The successive compression−expansion cycles of a mixture of OPESH and OPES-Au NPs exhibited a negligible hysteresis, which demonstrates the reversible mechanosensitive character of the self-assembly process. The corresponding distribution map of the normalized reflection intensities at successive cycles shows the reproducibility in the self-assembly of the interfacial film containing Au NPs (Figures 3c and S4). The recovery of the reflection band position and intensity of both molecular and nanocrystal components after two cycles demonstrates the high reversibility of OPES-Au NP self-assembly within the supramolecular phase. In contrast, no reversibility is observed for the analogous compression−expansion cycles of pure OPESH (inset in Figures 3b and S5), most likely due to strong intermolecular interactions. TEM micrographs of transferred films during the initial and final stages of the first compression show the transition from Au CCs to disk-shaped Au CMs (Figures 3d). This transition shows mechanosensitive reversibility due to an entropic contribution that may prevail under expansion at low Au NP surface concentrations. Although the degree of Au NP close-packing is similar to that obtained for the spontaneous formation of Au CMs (Figure 1d), improvements in the control of both the thickness (a single layer of Au NPs) and diameter (1−2 μm) dimensions are observed. We

DOI: 10.1021/jacs.6b09485
J. Am. Chem. Soc. 2017, 139, 1120−1128

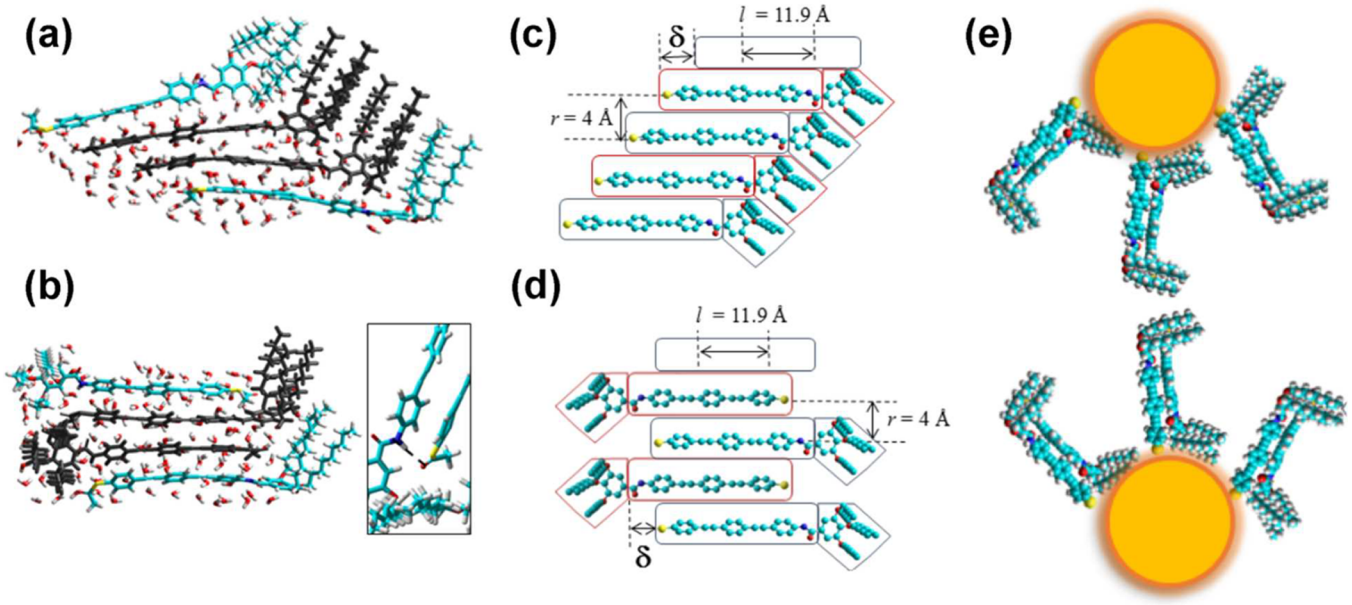

Figure 4. Proposed supramolecular arrangement of OPESH molecules on the basis of UV−vis reflection spectroscopy and molecular dynamics simulation data. (a,b) Final snapshots of monolayers of OPESH (side view) from the slipped and alternated configurations, respectively. The inset in (b) shows intermolecular H-bonding. Two OPESH molecules are depicted in black in each configuration to highlight their intermolecular interactions. Key color for atoms: H (white), C (cyan), O (red), N (blue), S (yellow). (c,d) Parameters for the extended dipole model showing the relative orientation of the OPESH molecules and their transition dipoles within the slipped and alternated configurations, respectively. (e) Schematics of the final supramolecular alternated dimers at the interparticle gap within Au CCs.

attribute the obtained monodispersity to the fine control of the area per molecule, and thus per Au NP, achieved with the Langmuir technique under compression and expansion conditions. After a complete cycle, a reversible transition from Au CMs to Au CCs is realized (Figure 3d), in good agreement with the characteristic absence of hysteresis observed in the surface pressure−area cyclic isotherms.

Quantitative Assessment of Supramolecular Arrangement. The interfacial self-assembly of the Au NPs within Au CMs is mediated by the supramolecular structuring of the OPESH molecule and triggered by the application of surface pressure as an external mechanical stimulus. A combination of computer simulations based on molecular dynamics and experimental measurements using *in situ* UV−vis reflection spectroscopy can be used to determine the supramolecular arrangement at the molecular level (the details of the computer simulations are described in Figures S8−S13).

UV−vis reflection spectroscopy at the liquid interface allows gathering *in situ* quantitative information on the orientation of the OPESH molecules at such interface, thus ruling out any reflection signal from the bulk solution. The normalized reflection is given by the following equation:

$$\Delta R_{\text{norm}} = A_{\text{chromophore}}\Delta R = \frac{2.303 \times 10^{17} f_0 \varepsilon}{N_A}\sqrt{R_S} = 5.41 \times 10^{-8} f_0 \varepsilon \quad (1)$$

where ΔR_{norm} represents the normalized UV−vis reflection signal, obtained as the product of the measured absolute UV−vis reflection signal by the molecular area of the chromophore, in this case the OPE group. ε and f_0 denote the absorption coefficient and an orientation factor accounting for a given preferred orientation of the transition dipoles, respectively. An f_0 value of ca. 1.5 was obtained in the case of OPESH assembly in the absence of Au NPs, indicating a parallel orientation of the transition dipole moments with respect to the interface.[44] For the current OPE ligands, the transition dipole moments and the main axis of the backbone are coincident, therefore the OPE units are parallel to the liquid interface. Concerning the orientation of the OPESH molecules directly linked to the Au NP surface, an average isotropic distribution (f_0 = 1) around the complete Au NP is expected (Scheme 1b). Therefore, the absorption of incoming UV−vis radiation from the OPESH molecule will be enhanced from the relative arrangement of the OPESH molecules on the air/water interface, and no net effect is expected from the relative orientation of the OPESH molecules on the Au NPs. Molecular dynamics simulations were thus performed with such parallel orientation of the OPE groups as an initial prerequisite. Two initial configurations were considered: configuration I, *slipped*, in which the OPESH molecules are parallel to each other, and configuration II, *alternated*, in which the OPESH molecules display an antiparallel configuration. H-bonding with water molecules and intermolecular H-bonding in the slipped configuration were found to be the main intermolecular interactions sustaining the supramolecular structure, as shown in Figure 4a,b.

The molecular arrangements for both configurations obtained in the simulations were quantitatively analyzed by applying the extended dipole model to the data obtained by UV−vis reflection experiments. This model establishes a quantitative relation between the relative geometry of the transition dipoles and the shift of the UV−vis reflection bands when aggregation occurs.[59] The position of the UV−vis band of the OPESH supramolecular aggregate (λ_N) with respect to isolated OPESH (λ_{mon}) can be calculated using

DOI: 10.1021/jacs.6b09485
J. Am. Chem. Soc. 2017, 139, 1120−1128

$$\lambda_N = \frac{\lambda_{mon} hc \times 10^7}{hc \times 10^7 + 4\sum_{i=2}^{N} J_{1i} \frac{(N+1-i)}{N}} \quad (2)$$

where h and c are the Planck's constant and speed of light in a vacuum, respectively, J_{1i} is the interaction energy between the dipoles corresponding to the reference molecule and each i molecule of the lineal aggregate, and N is the aggregation number, N = 2, 3, ... As shown in Figure 4c,d, the transition dipoles of the OPE groups are placed parallel to each other. The transition dipoles that oscillate in the same direction are coupled into a single optically active component, acting as the basic supramolecular unit in spectroscopic terms. The UV−vis spectrum of the sheet-like aggregates formed by OPESH in the absence of Au NPs shows an absorption maximum at 333 nm (Figure 2a,b). According to the extended dipole model, a supramolecular structure with N_∞ (infinite OPESH molecules forming the aggregate) and a translational displacement of δ = 0.6 nm would appear at λ_N = 333 nm, in excellent agreement with the experimental data. Therefore, the slipped configuration accounts for the shift in the UV−vis band in monolayers of pure OPESH. These results can be rationalized in terms of a significant steric hindrance between the alkyl chains of parallel-oriented OPESH molecules, leading to the mentioned displacement, as depicted in Figure 4a. In addition to the translational displacement, the appearance of a red-shifted shoulder at ca. 370 nm with regard to the monomer absorption (Figure 2b) is suggestive of a slightly twisted conformation of the OPE units, most likely to facilitate hydrogen bonding between neighboring units within the sheets, as observed for other hydrogen-bonded dye aggregates.[60,61]

The molecular packing of the OPESH units is significantly different in the presence of Au NPs, forming hybrid assemblies with Au NPs (Au CMs and Au CCs), as discussed above. Note that there is an excess of ca. 10^4 equivalents of OPESH molecules per single Au NP, yet the Au NPs impose a supramolecular structure on the aggregated domains of OPE around the nanocrystals as well as on Au NP-bound OPESH molecules. The UV−vis bands corresponding to the OPESH molecules are located at similar wavelengths (316 nm) regardless of the Au NPs aggregation state (Figure 2b). A null intermolecular displacement of δ = 0 is required in the extended dipole model for such wavelength value. The absence of intermolecular displacement can only be achieved in the alternated supramolecular structure described by molecular dynamics simulations, in which the alkyl chains are alternately pointing to opposite sides. Moreover, in such supramolecular structure, N = 2, i.e., although the supramolecular structure may contain a large number of stacked OPESH molecules, the basic coherent unit detected by UV−vis spectroscopy is a dimer of OPESH molecules. Therefore, the Au NP surrounding domains of OPESH units are initially formed by dimerization of free OPESH molecules driven by $\pi-\pi$ interactions between directionally opposed aromatic moieties (Figure 4d). As postulated previously and in good agreement with the interparticle gaps observed in Au CCs, such dimers are additionally stabilized by H-bonding involving the amide functional groups of antiparallel-arranged OPE fragments located at the surface of Au NPs (Figure 4e). Moreover, the significant contribution from the solvophobically driven interactions between alkyl chains is responsible for the alternated configuration. The formation of larger aggregates than dimers is likely hindered by the curvature of the Au NPs, leading to distorted interactions between the surface-bound OPESH molecules. Remarkably, this organization is extended through the entire film to free OPESH molecules, acting the Au NPs as topological nucleation points within the supramolecular phase.

Molecular Harvesting and Pressure-Controlled Release. As the ultimate goal, we explored the mechanosensitive response of Au CMs as host matrices to harvest and release hydrophobic molecules at the air/water interface through fluorescence spectroscopy. To that end, dyes with phenyl groups were selected to ensure supramolecular π-stacking interactions with the OPE backbones within the membranes (Figure S14). Au CMs were prepared under spontaneous conditions at the interface of a highly diluted solution of the hydrophobic dye BODIPY (1×10^{-7} M),[62,63] in which non-significant variations in the typical disk shape and sizes of the membranes were observed. The fluorescence microscopy image of such an interface shows blue emission from the Au CMs upon excitation with UV light (Figure 5a) due to the characteristic emission properties of OPE derivatives (Figures S15 and S16).[49] Interestingly, a weak blue emission is observed in the intermembrane region, confirming that OPESH molecules are mainly located at the Au CMs. The weak luminescence between NPs arises more likely from the fluorescence quenching observed for plasmonic NPs rather than from a preferred orientation of the OPESH molecules (see previous section). Concomitantly, green emission is observed from the Au CMs upon excitation with blue light (Figure 5b), thus confirming the ability of the superstructures to efficiently entrap BODIPY molecules. The observed emissions of both OPESH and BODIPY dyes do not change when a polarizer is used, thus confirming the random distribution of molecules

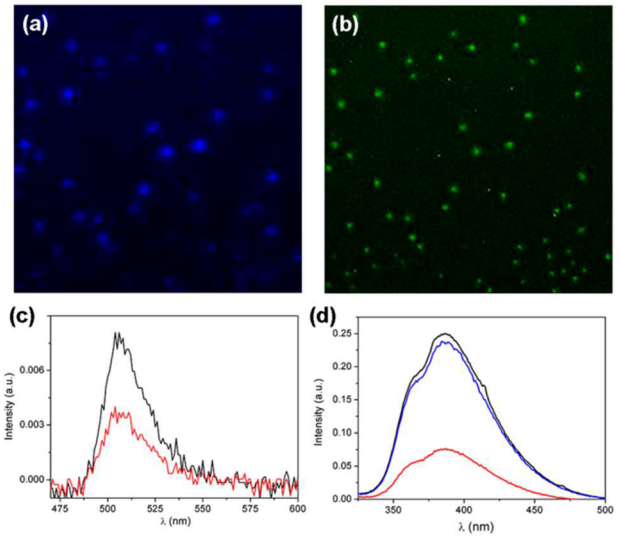

Figure 5. Molecular harvesting and pressure controlled release of mechanosensitive supramolecular gold colloidal membranes. (a,b) Optical fluorescence microscopy images at the liquid interface of Au CMs loaded with the highly hydrophobic dye BODIPY excited with UV light and recorded at the blue and green visible regions, respectively (21 μm × 21 μm). (c) Emission spectra of the BODIPY dye in bulk solution before (black) and after (red) preparation of the Au CMs (λ_{exc} = 460 nm). (d) Emission spectra of a dibenzofuran-derived pollutant in bulk solution in a compression (from black to red spectra) and expansion (recovery of the blue spectrum) cyclic experiment (from ~0 to 30 mN/m surface pressures).

DOI: 10.1021/jacs.6b09485
J. Am. Chem. Soc. 2017, 139, 1120−1128

within the Au CMs and the molecular isotropy of the membranes (Figure S17). Although quenching processes between the fluorophores and the Au NPs cannot be excluded, the observed intense fluorescence points to a low plasmonic efficiency of the selected Au NPs, in good agreement with their small nanocrystal size (10.5 ± 1.3 nm average in diameter).

Additionally, we determined the variation in the concentration of BODIPY in bulk solution during the spontaneous formation of Au CMs by steady-state fluorescence spectroscopy (Figure 5c). The presence of Au CMs induces a significant quenching (ca. 50%) of the BODIPY emission at 506 nm. This result shows that the formation of Au CMs strongly affects the concentration of hydrophobic molecules placed at the air/water interface by molecular trapping, thus shifting the equilibrium between hydrophobic molecules from the bulk solution to the air/water interface. The binding constant, K_b, between BODIPY and Au CMs was estimated to be 5.0×10^5 M^{-1} by a Langmuir isotherm model at 25 °C (Figure S18), which shows a high affinity between the guest and host species in comparison to conventional amphiphilic interfacial systems ($K_b \approx 1-10 \times 10^3$ M^{-1}),[64] pointing out the supramolecular character of the binding interactions.

The reversible mechanosensitive functionality of Au CMs was tested with a diluted solution (1×10^{-7} M) of a dibenzofuran derivative,[65] with a compression−expansion cyclic experiment, demonstrating the potential of the membranes as pollutant harvest/release systems. The emission intensity of the dibenzofuran bulk solution at 385 nm decreased by 70% at surface pressures from ∼0 to 30 mN/m during the transition from Au CCs to Au CMs as the open and closed configurations of the superstructures (Figure 5d). Finally, 95% of the intensity was recovered after the expansion cycle. Considering that >75% of dibenzofuran molecules may be initially placed at the air/water interface at such highly diluted conditions, we estimate that >90% of the pollutant was efficiently trapped and released during Au CM formation.

CONCLUSIONS

In conclusion, rational design of small, self-assembling π-conjugated ligands has been exploited to reversibly control the hierarchical self-assembly of gold nanoparticles into organized assemblies ranging from gold colloidal clusters to membranes at the air/water interface. The superstructures are maintained by cooperative non-covalent interactions between the π-conjugated molecules directly linking and surrounding the gold nanocrystals. The supramolecular phase in isolation displays a molecular arrangement (translationally slipped stacking) that is dramatically different from that in the presence of NPs (antiparallel packing). As the molecular arrangement remains constant during colloidal clustering, we thus conclude that Au NPs act as supramolecular nucleation points, imposing the observed organization. Reversible formation of the superstructures has been achieved for the first time through a dynamic mechanical stimulus, i.e., applying a given surface pressure through the Langmuir technique. Interestingly, this approach offers a methodology for obtaining mechanosensitive colloidal membranes by applying a surface pressure of ca. 30 mN/m, which is equivalent to the biological membrane pressure. Therefore, these artificial systems built up by smaller Au NP units can be potentially used for mimicking the mechanical behavior of biological membranes at the air/water interface. Moreover, the obtained colloidal membranes can act as reservoirs for highly hydrophobic molecules with relatively high binding constants ($K_b = 5.0 \times 10^5$ M^{-1}) in a reversible manner, thus trapping and releasing such molecules on demand.

Our novel methodology for fabricating reversible mechanosensitive colloidal membranes offers great potential to be extended to a wide range of nanoparticles and colloids, and provide a self-assembled nanotechnological platform for functional materials in environmental remediation, sensing, and biostructure mimicking.

ASSOCIATED CONTENT

Supporting Information

The Supporting Information is available free of charge on the ACS Publications website at DOI: 10.1021/jacs.6b09485.

Synthetic details, compound and nanoparticle characterizations, TEM, Langmuir experiments, UV−vis analyses and simulations, Brewster angle microscopy, molecular mechanics simulations, oscillator strength and extended dipole model calculations, and fluorescence microscopy, including Figures S1−S18 (PDF)

AUTHOR INFORMATION

Corresponding Authors

*jjginer@uco.es
*fernandg@uni-muenster.de
*aguerrero@quim.ucm.es

ORCID

David Ávila-Brande: 0000-0003-0452-2482
Andrés Guerrero-Martínez: 0000-0001-8576-2896

Notes

The authors declare no competing financial interest.

ACKNOWLEDGMENTS

We thank Laura R. Arriaga for stimulating discussions. This work has been funded by the Spanish MINECO (MAT2014-59678-R) and the Madrid Regional Government (S2013/MIT-2807). J.P.C. acknowledges receipt of a Ciencia sem Fronteiras fellowship from the CNPq of Brazil. J.J.G.-C. (#RyC-2014-14956) and A.G.-M. (#RyC-2011-08609) acknowledge receipt of a Ramón y Cajal Fellowship from the Spanish the Ministry of Economy and Competitiveness. G.F. thanks the Humboldt foundation for financial support (Sofja Kovalevskaja Programme). The facilities provided by the Nuclear Magnetic Resonance Center and National Center of Microscopy at Complutense University of Madrid are gratefully acknowledged.

REFERENCES

(1) Grzelczak, M.; Vermant, J.; Furst, E. M.; Liz-Marzán, L. M. *ACS Nano* **2010**, *4*, 3591.
(2) Guerrero-Martínez, A.; Grzelczak, M.; Liz-Marzán, L. M. *ACS Nano* **2012**, *6*, 3655.
(3) Fan, J. A.; Wu, C.; Bao, K.; Bao, J.; Bardhan, R.; Halas, N. J.; Manoharan, V. N.; Nordlander, P.; Shvets, G.; Capasso, F. *Science* **2010**, *328*, 1135.
(4) Dinsmore, A. D.; Hsu, M. F.; Nikolaides, M. G.; Marquez, M.; Bausch, A. R.; Weitz, D. A. *Science* **2002**, *298*, 1006.
(5) Lettinga, M. P.; Grelet, E. *Phys. Rev. Lett.* **2007**, *99*, 197802.
(6) Osterman, N.; Poberaj, I.; Dobnikar, J.; Frenkel, D.; Ziherl, P.; Babic, D. *Phys. Rev. Lett.* **2009**, *103*, 228301.
(7) Sharma, P.; Ward, A.; Gibaud, T.; Hagan, M. F.; Dogic, Z. *Nature* **2014**, *513*, 77.

DOI: 10.1021/jacs.6b09485
J. Am. Chem. Soc. 2017, 139, 1120−1128

(8) Kang, L.; Gibaud, T.; Dogic, Z.; Lubensky, T. C. *Soft Matter* **2016**, *12*, 386.
(9) Hudson, Z. M.; Lunn, D. J.; Winnik, M. A.; Manners, I. *Nat. Commun.* **2014**, *5*, 3372.
(10) Shevchenko, E. V.; Talapin, D. V.; Kotov, N. A.; O'Brien, S.; Murray, C. B. *Nature* **2006**, *439*, 55.
(11) Barry, E.; Dogic, Z. *Proc. Natl. Acad. Sci. U. S. A.* **2010**, *107*, 10348.
(12) Gibaud, T.; Barry, E.; Zakhary, M. J.; Henglin, M.; Ward, A.; Yang, Y.; Berciu, C.; Oldenbourg, R.; Hagan, M. F.; Nicastro, D.; Meyer, R. B.; Dogic, Z. *Nature* **2012**, *481*, 341.
(13) Bowden, N.; Choi, I. S.; Grzybowski, B. A.; Whitesides, G. M. *J. Am. Chem. Soc.* **1999**, *121*, 5373.
(14) Yang, M.; Chan, H.; Zhao, G.; Bahng, J. H.; Zhang, P.; Král, P.; Kotov, N. A. *Nat. Chem.* **2016**, DOI: 10.1038/nchem.2641.
(15) Ma, W.; Kuang, H.; Wang, L.; Xu, L.; Chang, W.-S.; Zhang, H.; Sun, M.; Zhu, Y.; Zhao, Y.; Liu, L.; Xu, C.; Link, S.; Kotov, N. A. *Sci. Rep.* **2013**, *3*, 1934.
(16) Herzig, E. M.; White, K. A.; Schofield, A. B.; Poon, W. C. K.; Clegg, P. S. *Nat. Mater.* **2007**, *6*, 966.
(17) White, S. J.; Heijne, G. V. *Curr. Opin. Struct. Biol.* **2004**, *14*, 397.
(18) Gottlieb, P. A.; Sachs, F. *Nature* **2012**, *483*, 163.
(19) Whitesides, G. M.; Mathias, J. P.; Seto, C. T. *Science* **1991**, *254*, 1312.
(20) Krieg, E.; Weissman, H.; Shirman, E.; Shimoni, E.; Rybtchinski, B. *Nat. Nanotechnol.* **2011**, *6*, 141.
(21) Qi, Z.; Traulsen, N. L.; Malo de Molina, P.; Schlaich, C.; Gradzielski, M.; Schalley, C. A. *Org. Biomol. Chem.* **2014**, *12*, 503.
(22) Hermans, T. M.; Broeren, M. A. C.; Gomopoulos, N.; van der Schoot, P.; van Genderen, M. H. P.; Sommerdijk, N. A. J. M.; Fytas, G.; Meijer, E. W. *Nat. Nanotechnol.* **2009**, *4*, 721.
(23) Du, C.; Falini, G.; Fermani, S.; Abbott, C.; Moradian-Oldak, J. *Science* **2005**, *307*, 1450.
(24) Bai, Y.; Luo, Q.; Liu, J. *Chem. Soc. Rev.* **2016**, *45*, 2756.
(25) Yao, Y.; Wang, Y.; Huang, F. *Chem. Sci.* **2014**, *5*, 4312.
(26) Coelho, J. P.; González-Rubio, G.; Delices, A.; Barcina, J. O.; Salgado, C.; Ávila, D.; Peña-Rodriguez, O.; Tardajos, G.; Guerrero Martínez, A. *Angew. Chem., Int. Ed.* **2014**, *53*, 12751.
(27) Aida, T.; Meijer, E. W.; Stupp, S. I. *Science* **2012**, *335*, 813.
(28) Coelho, J. P.; Tardajos, G.; Stepanenko, V.; Roedle, A.; Fernández, G.; Guerrero-Martínez, A. *ACS Nano* **2015**, *9*, 11241.
(29) Wakabayashi, R.; Endo, H.; Shinkai, S.; Ariga, K.; Takeuchi, M. *Dalton Trans.* **2013**, *42*, 15911.
(30) Meldrum, F. C.; Kotov, N. A.; Fendler, J. H. *Langmuir* **1994**, *10*, 2035.
(31) Kotov, N. A.; Meldrum, F. C.; Wu, C.; Fendler, J. H. *J. Phys. Chem.* **1994**, *98*, 2735.
(32) Kaiser, T. E.; Stepanenko, V.; Würthner, F. *J. Am. Chem. Soc.* **2009**, *131*, 6719.
(33) Yagai, S.; Seki, T.; Karatsu, T.; Kitamura, A.; Wuerthner, F. *Angew. Chem., Int. Ed.* **2008**, *47*, 3367.
(34) Ogi, S.; Sugiyasu, K.; Manna, S.; Samitsu, S.; Takeuchi, M. *Nat. Chem.* **2014**, *6*, 188.
(35) Rest, C.; Kandanelli, R.; Fernández, G. *Chem. Soc. Rev.* **2015**, *44*, 2543.
(36) van Herrikhuyzen, J.; George, S. J.; Vos, M. R. J.; Sommerdijk, N. A. J. M.; Ajayaghosh, A.; Meskers, S. C. J.; Schenning, A. P. H. J. *Angew. Chem., Int. Ed.* **2007**, *46*, 1825.
(37) Kumar, V. R. R.; Sajini, V.; Sreeprasad, T. S.; Praveen, V. K.; Ajayaghosh, A.; Pradeep, T. *Chem. - Asian J.* **2009**, *4*, 840.
(38) de Greef, T. F. A.; Smulders, M. M. J.; Wolffs, M.; Schenning, A. P. H. J.; Sijbesma, R. P.; Meijer, E. W. *Chem. Rev.* **2009**, *109*, 5687.
(39) Albert, S. K.; Thelu, H. V. P.; Golla, M.; Krishnan, N.; Chaudhary, S.; Varghese, R. *Angew. Chem., Int. Ed.* **2014**, *53*, 8352.
(40) Aparicio, F.; Nieto-Ortega, B.; Nájera, F.; Ramírez Aguilar, F. J.; López Navarrete, J. T.; Casado, J.; Sánchez, L. *Angew. Chem., Int. Ed.* **2014**, *53*, 1373.
(41) Garcia, F.; Sanchez, L. *J. Am. Chem. Soc.* **2012**, *134*, 734.
(42) Gopal, A.; Hifsudheen, M.; Furumi, S.; Takeuchi, M.; Ajayaghosh, A. *Angew. Chem., Int. Ed.* **2012**, *51*, 10505.
(43) Gopal, A.; Varghese, R.; Ajayaghosh, A. *Chem. - Asian J.* **2012**, *7*, 2061.
(44) Garcia, F.; Sanchez, L. *Chem. - Eur. J.* **2010**, *16*, 3138.
(45) Mahesh, S.; Thirumalai, R.; Yagai, S.; Kitamura, A.; Ajayaghosh, A. *Chem. Commun.* **2009**, 5984.
(46) Yagai, S.; Kubota, S.; Iwashima, T.; Kishikawa, K.; Nakanishi, T.; Karatsu, T.; Kitamura, A. *Chem. - Eur. J.* **2008**, *14*, 5246.
(47) Yagai, S.; Kubota, S.; Unoike, K.; Karatsu, T.; Kitamura, A. *Chem. Commun.* **2008**, 4466.
(48) Yagai, S.; Mahesh, S.; Kikkawa, Y.; Unoike, K.; Karatsu, T.; Kitamura, A.; Ajayaghosh, A. *Angew. Chem., Int. Ed.* **2008**, *47*, 4691.
(49) Bunz, U. H. F.; Seehafer, K.; Bender, M.; Porz, M. *Chem. Soc. Rev.* **2015**, *44*, 4322.
(50) Allampally, N. K.; Mayoral, M. J.; Chansai, S.; Lagunas, M. C.; Hardacre, C.; Stepanenko, V.; Albuquerque, R. Q.; Fernández, G. *Chem. - Eur. J.* **2016**, *22*, 7810.
(51) Orsi, D.; Cristofolini, L.; Baldi, G.; Madsen, A. *Phys. Rev. Lett.* **2012**, *108*, 105701.
(52) Van Duyne, P. R. *Science* **2004**, *306*, 985.
(53) Prodan, E.; Radloff, C.; Halas, N. J.; Nordlander, P. A. *Science* **2003**, *302*, 419.
(54) Spano, F. C.; Silva, C. *Annu. Rev. Phys. Chem.* **2014**, *65*, 477.
(55) Spano, F. C. *Acc. Chem. Res.* **2010**, *43*, 429.
(56) Kasha, M.; Rawls, H. R.; El-Bayoumi, M. A. *Pure Appl. Chem.* **1965**, *11*, 371.
(57) Campolongo, M. J.; Tan, S. J.; Smilgies, D. M.; Zhao, M.; Chen, Y.; Xhangolli, I.; Cheng, W.; Luo, D. *ACS Nano* **2011**, *5*, 7978.
(58) Guzmán, E.; Liggieri, L.; Santini, E.; Ferrari, M.; Ravera, F. *J. Phys. Chem. C* **2011**, *115*, 21715.
(59) Rubia-Payá, C.; de Miguel, G.; Martín-Romero, M. T.; Giner-Casares, J.; Camacho, L. *Adv. Colloid Interface Sci.* **2015**, *225*, 134.
(60) Rödle, A.; Ritschel, B.; Mück-Lichtenfeld, C.; Stepanenko, V.; Fernandez, G. *Chem. - Eur. J.* **2016**, *22*, 15772.
(61) Li, X.-Q.; Stepanenko, V.; Chen, Z.; Prins, P.; Siebbeles, L. D. A.; Würthner, F. *Chem. Commun.* **2006**, 3871.
(62) Treibs, A.; Kreuzer, F.-H. *Liebigs Ann. Chem.* **1968**, *718*, 208.
(63) Chu, G. M.; Guerrero-Martínez, A.; Ramírez de Arellano, C.; Fernández, I.; Sierra, M. A. *Inorg. Chem.* **2016**, *55*, 2737.
(64) Beschiaschvili, G.; Seelig, J. *Biochemistry* **1990**, *29*, 10995.
(65) Sainz-Rozas, P. R.; Isasi, J. R.; Sánchez, M.; Tardajos, G.; González-Gaitano, G. *J. Phys. Chem. A* **2004**, *108*, 392.

DOI: 10.1021/jacs.6b09485
J. Am. Chem. Soc. 2017, 139, 1120−1128